8-15-1984

Three-reflection halfwave and quarterwave retarders using dielectric-coated metallic mirrors

T. F. Thonn

R. M.A. Azzam
University of New Orleans, razzam@uno.edu

Recommended Citation

T. F. Thonn and R. M. A. Azzam, "Three-reflection halfwave and quarterwave retarders using dielectric-coated metallic mirrors," Appl. Opt. 23, 2752-2759 (1984)

Three-reflection halfwave and quarterwave retarders using dielectric-coated metallic mirrors

T. F. Thonn and R. M. A. Azzam

A design procedure is described to determine the thicknesses of single-layer coatings of a given dielectric on a given metallic substrate so that a specified net phase retardance (and/or a net relative amplitude attenuation) between the p and s polarizations is achieved after three reflections from a symmetrical arrangement of three mirrors that maintain collinearity of the input and output beams. Examples are presented of halfwave and quarterwave retarders (HWR and QWR) that use a ZnS–Ag film–substrate system at the CO_2-laser wavelength $\lambda = 10.6$ μm. The equal net reflectances for the p and s polarizations are computed and found to be high (above 90%) for most designs. Sensitivity of the designs (deviation of the magnitude and phase of the ratio of net complex p and s reflection coefficients from design specifications) to small film-thickness and angle-of-incidence errors is examined, and useful operation over a small wavelength range (10–11 μm) is demonstrated.

I. Introduction

An external reflection retarder is a device that introduces a relative phase shift between the parallel p and perpendicular s polarization components of incident monochromatic light without affecting their relative amplitudes.[1] The design of such single-reflection retarders using optically isotropic film–substrate systems has been amply described and applied.[2–7] Single-reflection multilayer-coated retarders have also been reported.[8–10]

In this paper we describe the design of three-reflection film–substrate retarders that maintain collinearity of the input and output beams (Fig. 1). In such systems, the individual reflections are not retarding, but the combined net effect of all three reflections produces the desired differential phase shift and equal amplitude attenuation for the p and s polarizations. The method is applied to halfwave and quarterwave retarders (HWR and QWR) that use ZnS–Ag (film–substrate) mirrors at the CO_2-laser wavelength $\lambda = 10.6$ μm. The sensitivity of these designs to small film-thickness and angle-of-incidence errors is examined, and useful operation over a small wavelength range (10–11 μm) is demonstrated.

The authors are with University of New Orleans, Department of Electrical Engineering, Lakefront, New Orleans, Louisiana 70148.

Received 16 April 1984.
0003-6935/84/162752-08$02.00/0.

II. Design Procedure

We consider a symmetrical three-mirror system (Fig. 1), where the angles of incidence ϕ_1, ϕ_2, and ϕ_3 are interrelated as follows:

$$\phi_3 = \phi_1, \tag{1}$$

$$\phi_2 = 2\phi_1 - 90°. \tag{2}$$

Equation (2) shows that ϕ_1 must be >45°. We assume an air (or vacuum) ambient of refractive index $N_0 = 1$, a transparent film of refractive index N_1, and an absorbing metallic substrate of complex refractive index N_2 for each and all mirrors.

The change of polarization on single reflection from an optically isotropic surface is completely determined by the ratio of complex reflection coefficients,

$$\rho = R_p/R_s, \tag{3}$$

of the parallel p and perpendicular s polarizations. For light of wavelength λ, incident at an angle ϕ from a transparent ambient onto a metallic substrate coated by a dielectric film of thickness d, the p and s reflection coefficients are given by[11]

$$R_\nu = \frac{r_{01\nu} + r_{12\nu}\exp(-j2\pi\zeta)}{1 + r_{01\nu}r_{12\nu}\exp(-j2\pi\zeta)}, \quad \nu = p,s. \tag{4}$$

$r_{01\nu}$ and $r_{12\nu}$ are the ambient–film and film–substrate Fresnel's interface reflection coefficients for the ν polarization, and ζ is the normalized film thickness:

$$\zeta = d/D_\phi, \tag{5}$$

where

$$D_\phi = \frac{\lambda}{2}(N_1^2 - N_0^2\sin^2\phi)^{-1/2} \tag{6}$$

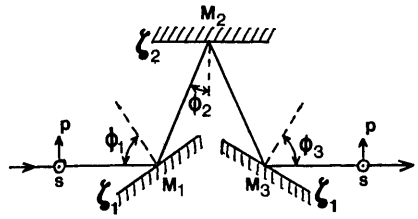

Fig. 1. Three-mirror reflection system.

is the film-thickness period. From Eqs. (3) and (4) we see that ρ is a function of ϕ and ζ:

$$\rho = f(\phi,\zeta). \tag{7}$$

We require that all mirrors be made of the same metallic substrate coated by a transparent thin film of the same dielectric material and of the same thickness ζ_1 for mirrors M_1 and M_3 but of a different thickness ζ_2 for mirror M_2. Then we follow a procedure that parallels that described previously by Azzam and Khan.[12]

The net effect of three reflections is given by the product

$$\rho_n = \rho_1\rho_2\rho_3 = f^2(\phi_1,\zeta_1)f(\phi_2,\zeta_2). \tag{8}$$

The ratio of net complex p and s reflection coefficients can be written

$$\rho_n = |\rho_n| \exp(j\Delta_n). \tag{9}$$

where

$$|\rho_n| = |R_{pn}|/|R_{sn}|, \tag{10a}$$

$$\Delta_n = \delta_{pn} - \delta_{sn}, \tag{10b}$$

are the net relative amplitude attenuation and the difference between the net phase shifts experienced by the p and s polarization components, respectively. For a given ρ_n the following equation must be solved for ζ_1,ζ_2:

$$f(\phi_2,\zeta_2) = g(\phi_1,\zeta_1), \tag{11}$$

where

$$g(\phi_1,\zeta_1) = \rho_n/f^2(\phi_1,\zeta_1). \tag{12}$$

Equation (11) can be solved for given ϕ_1 and ϕ_2 using the Newton-Raphson iteration method[13] on a digital computer. Equation (11) is broken into its real and imaginary parts:

$$f_r(\phi_2,\zeta_2) = g_r(\phi_1,\zeta_1), \tag{13a}$$

$$f_i(\phi_2,\zeta_2) = g_i(\phi_1,\zeta_1), \tag{13b}$$

where

$$f = f_r + jf_i, \qquad g = g_r + jg_i. \tag{14}$$

We look for solutions ζ_1,ζ_2 of Eqs. (13) in the reduced thickness range:

$$0 \le \zeta_{1,2} < 1. \tag{15}$$

An arbitrary initial trial solution (ζ_1^0,ζ_2^0) is assumed that will be incremented by $(\Delta\zeta_1,\Delta\zeta_2)$ to move closer to the correct solution. The new vector $(\zeta_1^0 + \Delta\zeta_1,\zeta_2^0 + \Delta\zeta_2)$ is then required to satisfy Eqs. (13):

$$f_r(\phi_2,\zeta_2^0 + \Delta\zeta_2) = g_r(\phi_1,\zeta_1^0 + \Delta\zeta_1), \tag{16a}$$

$$f_i(\phi_2,\zeta_2^0 + \Delta\zeta_2) = g_i(\phi_1,\zeta_1^0 + \Delta\zeta_1). \tag{16b}$$

The initial vector is assumed to be sufficiently close to the correct solution to justify a linear two-term Taylor-series expansion of Eqs. (16); this gives

$$f_r'(\phi_2,\zeta_2^0)\Delta\zeta_2 - g_r'(\phi_1,\zeta_1^0)\Delta\zeta_1 = g_r(\phi_1,\zeta_1^0) - f_r(\phi_2,\zeta_2^0), \tag{17a}$$

$$f_i'(\phi_2,\zeta_2^0)\Delta\zeta_2 - g_i'(\phi_1,\zeta_1^0)\Delta\zeta_1 = g_i(\phi_1,\zeta_1^0) - f_i(\phi_2,\zeta_2^0). \tag{17b}$$

In Eqs. (17) the prime superscript indicates the first partial derivative with respect to ζ (i.e., $f_r' = \partial f_r/\partial\zeta$ etc). These derivatives are obtained from Eqs. (3) and (4) as follows:

$$f' = \rho' = (R_p'/R_s) - (R_pR_s'/R_s^2), \tag{18}$$

$$R_\nu' = -j2\pi \exp(-j2\pi\zeta)\frac{r_{12\nu}(1 - r_{01\nu}^2)}{[1 + r_{01\nu}r_{12\nu}\exp(-j2\pi\zeta)]^2}, \quad \nu = p,s, \tag{19}$$

$$g' = -2\rho_n f'/f^3, \tag{20}$$

$$f_r' = \mathrm{Re}f', f_i' = \mathrm{Im}f'; g_r' = \mathrm{Re}g', g_i' = \mathrm{Im}g'. \tag{21}$$

The two linear algebraic equations (17) are solved for $\Delta\zeta_1,\Delta\zeta_2$. The new vector $(\zeta_1^0 + \Delta\zeta_1,\zeta_2^0 + \Delta\zeta_2)$ is determined and used as the improved initial vector for the next round of iteration. This process is repeated until the changes of $\Delta\zeta_1,\Delta\zeta_2$ between iteration steps both fall below 10^{-6}, at which point the solution is considered reached. As a check, the final solution vector (ζ_1,ζ_2) is substituted into the right-hand side of Eq. (8), and ρ_n is verified to be the desired ρ_n.

The design procedure is general and can be applied at any wavelength to any film–substrate system and for any desired net ratio of complex reflection coefficients ρ_n. However, for any given combination of parameters and angle of incidence ϕ_1, no solution, one solution, or multiple solutions may exist. Thus it was necessary to plot, in the complex plane, the closed contours of ρ_2 and ρ_n/ρ_1^2 at given ϕ_1 (as ζ_1 and ζ_2 vary from 0 to 1) to verify the number of solutions (points of intersection) before doing the actual iteration.

We have found the above-described Newton-Raphson method to be adequate and that it converges after a reasonable number of iterations (usually <40), when an initial vector sufficiently close to the solution vector is chosen. All multiple solutions could be found by beginning iteration from different initial vectors.

Note that if (ζ_1,ζ_2) is a solution, $(\zeta_1 + m,\zeta_2 + n)$ will also be a solution, where m and n are any two positive integers. This follows from the fact that R_p, R_s, and ρ are periodic functions of ζ with period 1, as can be seen from Eqs. (3) and (4). The actual thicknesses of the film on mirrors M_1, M_3, and M_2 are then given by

$$(d_1,d_2) = (\zeta_1 D_{\phi 1},\zeta_2 D_{\phi 2}). \tag{22}$$

The net intensity reflectances of the three-mirror system can be calculated from Eq. (4) as

$$\mathcal{R}_{\nu n} = |R_{\nu 1}|^2|R_{\nu 2}|^2|R_{\nu 3}|^2, \qquad \nu = p \text{ or } s, \tag{23}$$

where $R_{\nu i}$ is the reflection coefficient for the ν polarization of mirror M_i (note that $R_{\nu 1} = R_{\nu 3}$ by design). In

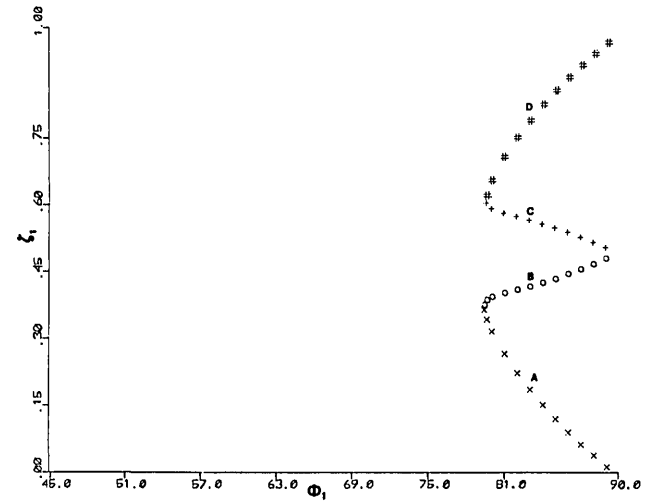

Fig. 2. Normalized film thickness ζ_1 required for HWR ($|\rho_n| = 1$, $\Delta_n = \pm 180°$) vs angle of incidence ϕ_1 (deg) in a ZnS–Ag three-reflection system at $\lambda = 10.6$ μm.

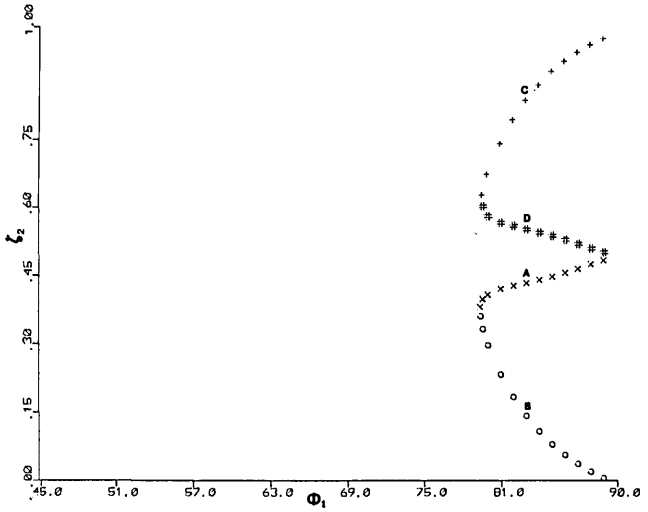

Fig. 3. Same as in Fig. 2 for the associated normalized film thickness ζ_2.

this paper, we consider only pure retarders, i.e., $|\rho_n| = 1$ and

$$\mathcal{R}_{pn} = \mathcal{R}_{sn}. \tag{24}$$

High values of $\mathcal{R}_{\nu n}$ are achieved when the substrate is metallic.

In the following examples, we will also examine the sensitivity of a design to small film-thickness and angle-of-incidence errors and to small wavelength changes. This is done by direct calculation of ρ_n from Eq. (8) with the design parameters perturbed by the corresponding error, namely, $\Delta d_1 = \Delta d_2 (\Delta \zeta_i = \Delta d_i / D_{\phi i})$, $\Delta \phi_1 = \Delta \phi_2$, or $\Delta \lambda$. The deviation from the desired ρ_n is expressed in terms of separate magnitude and phase errors:

$$\text{magnitude error} = |\rho_n| - 1,$$
$$\text{phase error} = \Delta_n - \Delta_{nd}, \tag{25}$$

where Δ_{nd} is the desired retardance. Wavelength sensitivity is computed neglecting the effect of material dispersion over the test range. Thus the wavelength shift $\Delta\lambda$ has the same effect as simultaneous film-thickness errors Δd_i so that $\Delta d_i / d_i = \Delta\lambda/\lambda$ and $i = 1,2,3$ for the respective mirror.

III. ZnS–Ag Halfwave Retarders at $\lambda = 10.6$ μm

As a first example, we have designed three-reflection halfwave retarders at the CO_2-laser wavelength $\lambda = 10.6$ μm using mirrors that consist of a transparent film of ZnS ($N_1 = 2.2$) on a Ag substrate ($N_2 = 9.5 - j73$)[8] in an air ambient ($N_0 = 1$).

The design procedure of Sec. II was applied with $|\rho_n| = 1$ and $\Delta_n = \pm 180°$ (HWR) at discrete angles of incidence ϕ_1 over the full range $45° < \phi_1 < 90°$. Figures 2 and 3 give the solutions for the normalized film thicknesses ζ_1 and ζ_2 plotted vs ϕ_1.

Table I lists a summary of the HWR design results for two angles of incidence: 80 and 85°. The table gives the normalized film-thickness solution pairs (ζ_1, ζ_2), film-thickness periods $D_{\phi 1}$ and $D_{\phi 2}$, the net reflectance $\mathcal{R}_{\nu n} (\nu = p,s)$, and the net phase shifts δ_{pn} and δ_{sn} experienced by the p and s components of polarization, respectively. From Figs. 2 and 3 we see that solutions exist only in the limited range $79.4° \leq \phi_1 < 90°$. Within

Table I. Summary of Design Results for ZnS–Ag Three-Reflection Halfwave Retarders (HWR: $|\rho_n| = 1$, $\Delta_n = \delta_{pn} - \delta_{sn} = \pm 180°$) at Two Angles of Incidence and for Wavelength $\lambda = 10.6$ μm [a]

ϕ_1	ζ_1	ζ_2	$D_{\phi 1}$	$D_{\phi 2}$	$\mathcal{R}_{\nu n}$	δ_{pn}	δ_{sn}
80 *A*	0.31634	0.40638	2.6941	2.6644	0.9672	−96.965	83.035
B	0.39404	0.29610	2.6941	2.6644	0.9689	−89.782	90.218
C	0.59110	0.67256	2.6941	2.6644	0.9689	91.178	−88.822
D	0.65557	0.58024	2.6941	2.6644	0.9675	97.402	−82.598
85 *A*	0.11938	0.44629	2.7020	2.6941	0.9557	−67.599	112.401
B	0.43494	0.07680	2.7020	2.6941	0.9627	−58.252	121.748
C	0.54840	0.90090	2.7020	2.6941	0.9629	58.296	−121.704
D	0.85867	0.53708	2.7020	2.6941	0.9560	67.523	−112.477

[a] ϕ_1 is the angle of incidence in degrees on mirrors M_1 and M_3; (ζ_1, ζ_2) is the normalized film-thickness solution pair; $D_{\phi i}$ is the film-thickness period in microns at ϕ_i, $i = 1,2$; $\mathcal{R}_{\nu n}$ is the net reflectance of the retarder for both polarizations ($\nu = p,s$); and δ_{pn}, δ_{sn} are the net phase shifts for the p and s polarizations in degrees. The refractive indices of ZnS and AG at 10.6 μm are taken to be 2.2 and 9.5–j73, respectively.

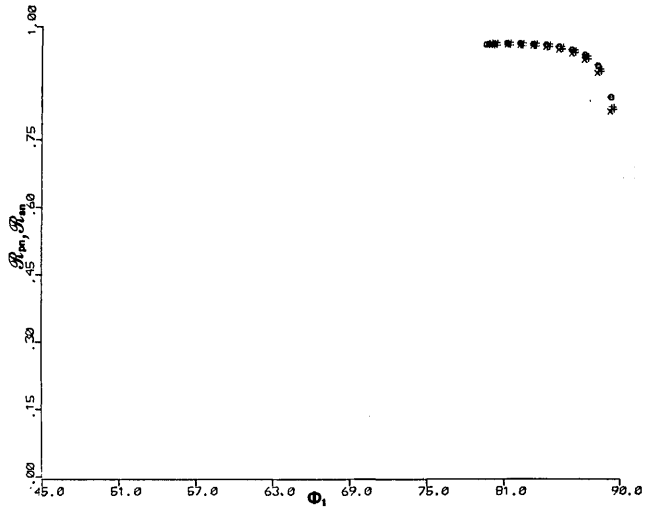

Fig. 4. Net intensity reflectances $\mathcal{R}_{pn} = \mathcal{R}_{sn}$ associated with the design solution pairs (ζ_1,ζ_2) of Figs. 2 and 3.

Table II. Magnitude and Phase Errors Caused by Introducing (I) Film-Thickness Errors ($\Delta d_1 = \Delta d_2 = \pm 1$ nm), (II) Angle-of-Incidence Errors ($\Delta\phi_1 = \Delta\phi_2 = \Delta\phi_3 = \pm 0.5°$) to the HWR Designs of Table I

Error type	ϕ_1 (deg)	Magnitude error $(\lvert\rho_n\rvert - 1) \times 10^4$ −	+	Phase error $(\Delta_n \mp 180°)$ (deg) −	+
I	80 *A*	−1.010	1.018	−0.0613	0.0633
	B	−1.017	1.027	−0.0577	0.0597
	C	1.007	−0.999	−0.0597	0.0578
	D	0.990	−0.985	−0.0626	0.0607
	85 *A*	−3.345	3.380	−0.0865	0.0927
	B	−2.536	2.586	−0.0714	0.0766
	C	2.567	−2.525	−0.0761	0.0713
	D	3.346	−3.310	−0.0921	0.0859
II	80 *A*	−2.061	2.088	6.0568	−6.1141
	B	1.385	−1.430	6.1212	−6.1799
	C	1.188	−1.230	−6.1639	6.2222
	D	−1.777	1.797	−6.0734	6.1299
	85 *A*	−6.922	8.039	12.1470	−12.5933
	B	15.510	−15.953	8.7586	−9.0116
	C	15.306	−15.745	−8.8312	9.0848
	D	−6.934	8.030	−12.1470	12.5889

this range we see four distinct solution pairs (branches *A*,*B*,*C*,*D*) that achieve HWR for each ϕ_1.

Figures 2 and 3 are nearly symmetrical with respect to the line $\zeta_{1,2} = 0.5$ due to the near symmetry of the constant-angle-of-incidence contours (CAIC) in the complex ρ plane with respect to the real axis.[2] Table I also indicates that for each thickness–solution pair that gives a net relative phase shift $\Delta_n = 180°$ there exists a corresponding solution that gives the equivalent retardance $\Delta_n = -180°$, so that $\zeta_A + \zeta_D \simeq 1$, $\zeta_B + \zeta_C \simeq 1$ (because the $\zeta = 0$ point on the CAIC is almost on the real axis).

Figure 4 gives a plot of the net intensity reflectance $\mathcal{R}_{vn}$ for both polarizations vs ϕ_1 for the solution pairs of Figs. 2 and 3. From Fig. 4 and Table I we see that $\mathcal{R}_{vn}$ is nearly the same for all solutions at a specific ϕ_1. $\mathcal{R}_{vn}$ decreases as ϕ_1 increases, first slowly then rapidly near $\phi_1 = 90°$, but remains high (>90%) for all angles of incidence ≤88°.

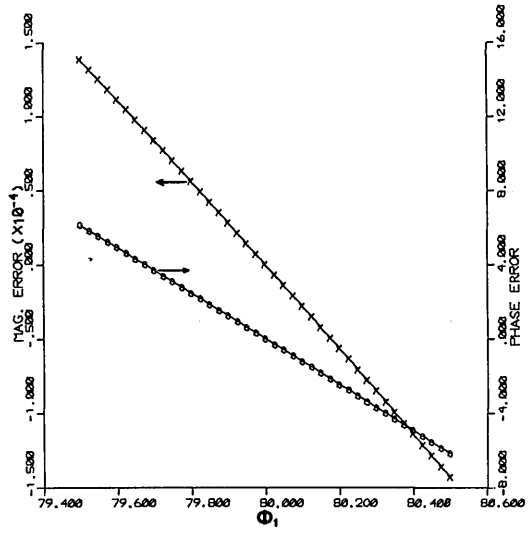

Fig. 5. Magnitude error ($|\rho_n| - 1$) and phase error [$\Delta_n - (180°)$] caused by angle-of-incidence $\Delta\phi_1 = \Delta\phi_2 = \Delta\phi_3 = \pm 0.5°$ for solution pair *B* at $\phi_1 = 80°$ of Table I.

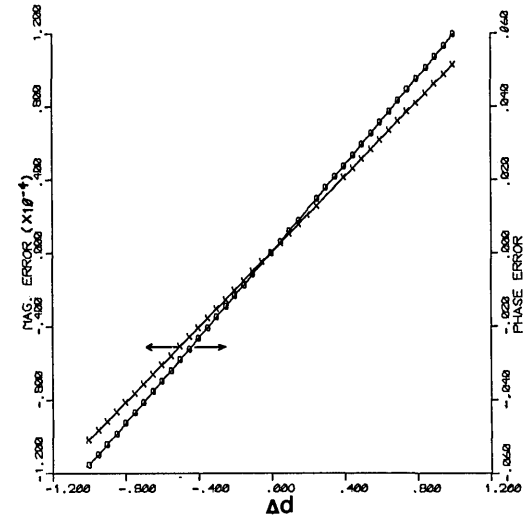

Fig. 6. Same as in Fig. 5 for $\Delta d_1 = \Delta d_2 = \pm 1$-nm changes of actual film thickness d_1 and d_2.

Table II gives the magnitude and phase errors generated by thickness errors $\Delta d_1 = \Delta d_2 = \pm 1$ nm and angle-of-incidence errors $\Delta\phi_1 = \Delta\phi_2 = \Delta\phi_3 = \pm 0.5°$. The errors at 85° are higher than those for the 80° designs.

Figures 5 and 6 show that these magnitude and phase errors vary essentially linearly with $\Delta\phi_i$ between ±0.5° and with Δd_i between ±1 nm for a specific design (solution *B* at $\phi_1 = 80°$).

Figure 7 shows the magnitude and phase errors that result when the wavelength λ scans the range 10 μm ≤ $\lambda \leq 11$ μm about the design wavelength $\lambda = 10.6$ μm for the same solution *B* at $\phi_1 = 80°$, neglecting the effect of material dispersion. Over this 1-μm wide spectral band, the system operates satisfactorily as a HWR with the magnitude error <1% and phase error <5%.

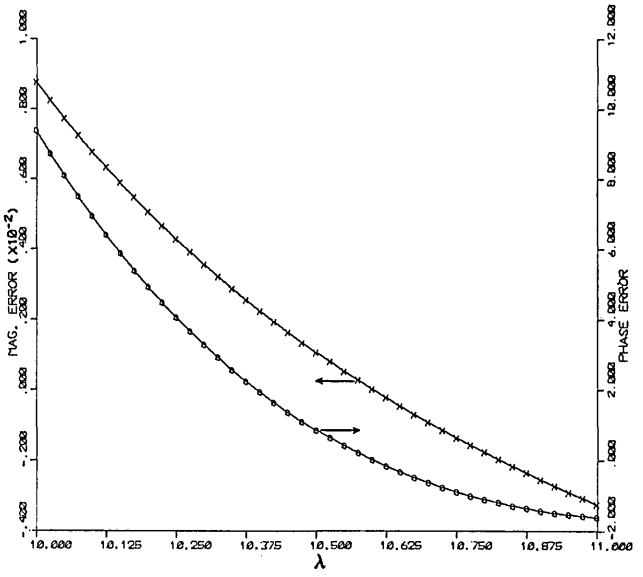

Fig. 7. Same as in Fig. 5 for wavelength changes in the range 10 μm $\leq \lambda \leq$ 11 μm.

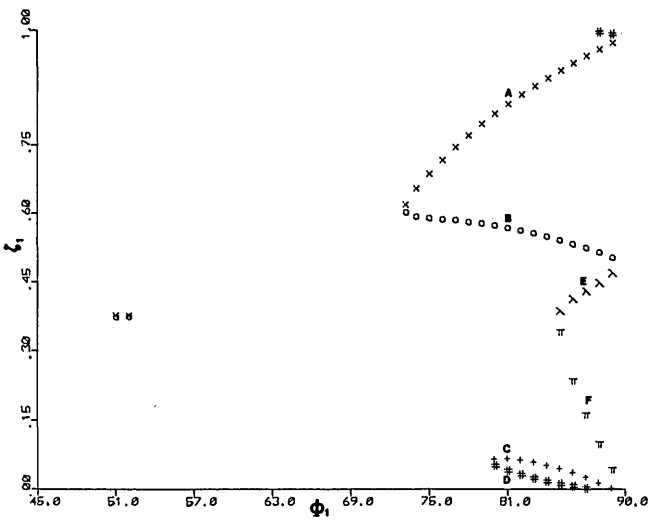

Fig. 8. Normalized film thickness ζ_1 required for QWR ($|\rho_n| = 1$, $\Delta_n = 90°$) vs angle of incidence ϕ_1 (deg) in a ZnS–Ag three-reflection system at $\lambda = 10.6$ μm.

IV. ZnS–Ag Quarterwave Retarders at $\lambda = 10.6$ μm

A. $\rho_n = +j$ Quarterwave Retarders (p Fast Axis)

We again assume mirrors that consist of a ZnS film on an Ag substrate at 10.6 μm with the same optical constants given in Sec. III.

The design procedure of Sec. II was applied with $|\rho_n| = 1$ and $\Delta_n = 90°$ (QWR) at discrete angles ϕ_1 in the range $45° < \phi_1 < 90°$. Figures 8 and 9 give the solutions for ζ_1 and ζ_2 plotted vs ϕ_1. Table III summarizes QWR design results for three angles of incidence: 52, 75, and 85°. From Figs 8 and 9 we see that multiple solutions at a specific ϕ_1 exist as follows. Two solutions are available in the ranges $51° \leq \phi_1 \leq 52°$ and $73.2° \leq \phi_1 \leq 79°$, four in the range $80° \leq \phi_1 \leq 84°$, and six solutions in the range $85° \leq \phi_1 < 90°$.

In Fig. 10 the net intensity reflectance $\mathcal{R}_{vn}$ is plotted vs ϕ_1 for the solutions of Figs. 8 and 9. $\mathcal{R}_{vn}$ is high for most solutions except near grazing incidence ($\phi_1 = 90°$) where it falls off rapidly.

Table IV shows the magnitude and phase errors caused by $\Delta d_i = \pm 1$-nm thickness errors and $\Delta\phi_i =$

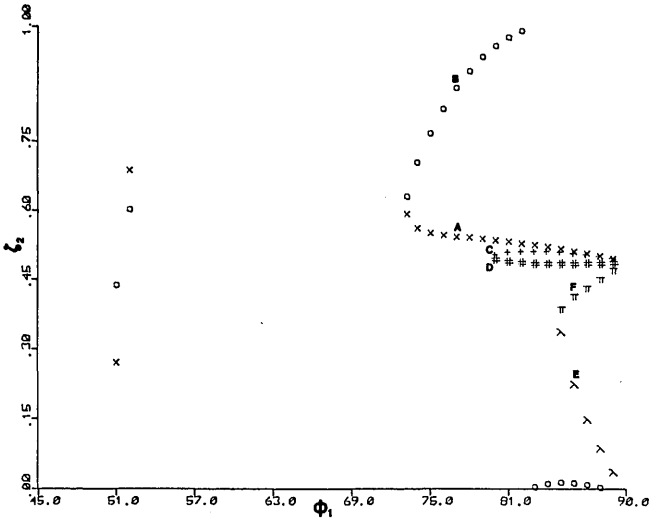

Fig. 9. Same as in Fig. 2 for the associated normalized film thickness ζ_2.

Table III. Summary of Design Results for ZnS–Ag Three-Reflection Quarterwave Retarders with p Fast Axis (QWR: $|\rho_n| = 1$, $\Delta_n = \delta_{pn} - \delta_{sn} = 90°$) at Three Angles of Incidence and for Wavelength $\lambda = 10.6$ μm [a]

ϕ_1	ζ_1	ζ_2	$D_{\phi 1}$	$D_{\phi 2}$	$\mathcal{R}_{vn}$	δ_{pn}	δ_{sn}
52 *A*	0.37716	0.68985	2.5751	2.4238	0.9445	178.381	88.381
B	0.37578	0.60396	2.5751	2.4238	0.9368	−143.182	126.818
75 *A*	0.68770	0.55294	2.6814	2.6207	0.9541	55.070	−34.930
B	0.59026	0.77066	2.6814	2.6207	0.9617	22.095	−67.905
85 *A*	0.91588	0.51795	2.7020	2.6941	0.9188	5.903	−84.097
B	0.54189	0.01364	2.7020	2.6941	0.9541	−28.401	−118.401
C	0.04588	0.51154	2.7020	2.6941	0.9001	17.318	−72.682
D	0.01175	0.48696	2.7020	2.6941	0.8578	108.005	18.005
E	0.38691	0.33921	2.7020	2.6941	0.9831	−138.976	131.024
F	0.34169	0.38882	2.7020	2.6941	0.9830	−139.512	130.488

[a] See footnote of Table I for explanation of notation.

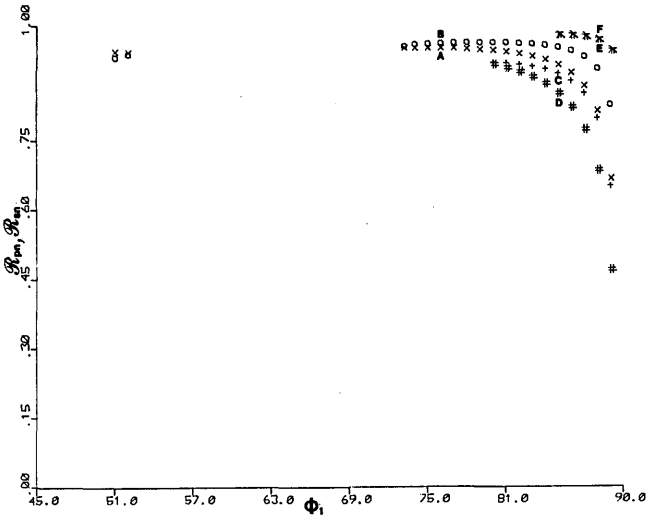

Fig. 10. Net intensity reflectances $\mathcal{R}_{pn} = \mathcal{R}_{sn}$ associated with the design solution pairs (ζ_1,ζ_2) of Figs. 8 and 9.

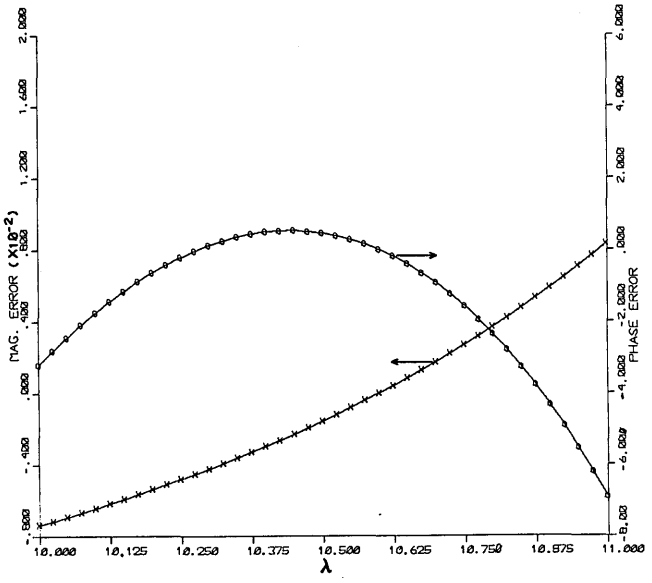

Fig. 11. Magnitude error ($|\rho_n| - 1$) and phase error ($\Delta_n - 90°$) caused by wavelength changes in the range 10 μm $\leq \lambda \leq$ 11 μm for solution pair B at $\phi_1 = 75°$ of Table III.

Table IV. Magnitude and Phase Errors Caused by Introducing (I) Film-Thickness Errors ($\Delta d_1 = \Delta d_2 = \pm 1$ nm), (II) Angle-of-Incidence Errors ($\Delta\phi_1 = \Delta\phi_2 = \Delta\phi_3 = \pm 0.5°$) to the QWR Designs of Table III

Error type	ϕ_1 (deg)	Magnitude error $(\lvert\rho_n\rvert - 1) \times 10^4$ −	+	Phase Error $(\Delta_n - 90°)$ (deg) −	+
I	52 *A*	−0.603	0.608	−0.0537	0.0550
	B	−0.573	0.576	−0.0546	0.0557
	75 *A*	1.072	−1.067	−0.0817	0.0797
	B	1.101	−1.092	−0.0682	0.0660
	85 *A*	7.479	−7.417	−0.1746	0.1609
	B	2.988	−2.916	−0.0943	0.0884
	C	3.982	−3.949	−0.2133	0.2046
	D	−5.518	5.314	−0.3010	0.3106
	E	−0.575	0.579	−0.0330	0.0341
	F	−0.571	0.575	−0.0333	0.0344
II	52 *A*	−0.093	0.094	1.9350	−1.9622
	B	−0.206	0.213	1.9246	−1.9512
	75 *A*	−2.734	2.850	−5.1858	5.2592
	B	1.402	−1.483	−5.0627	5.1303
	85 *A*	−4.169	7.389	−14.0402	15.2408
	B	24.356	−26.014	−5.7013	5.7001
	C	0.813	2.351	8.0346	−9.1883
	D	20.245	−25.010	7.1403	−8.4625
	E	0.842	−0.858	6.6376	−6.6682
	F	−1.007	1.000	6.5501	−6.5804

±0.5° angle-of-incidence errors. Again we see a general increase in these errors with ϕ_1. Although not shown here, we have also verified that for these designs the magnitude and phase errors vary essentially linearly with Δd_i between ±1 nm and with $\Delta\phi_i$ between ±0.5°, as expected.

Figure 11 shows the magnitude and phase errors that result when the wavelength λ scans the range 10 μm $\leq \lambda \leq$ 11 μm for solution B at $\phi_1 = 75°$. Again the effect of material dispersion is neglected. The magnitude error remains <1% and the phase error <8%, indicating acceptable performance as a QWR over this spectral range.

B. $\rho_n = -j$ Quarterwave Retarders (s Fast Axis)

The ZnS–Ag film–substrate system is assumed with optical constants at 10.6 μm given in Sec. III, as before.

The design procedure of Sec. II was applied with $|\rho_n| = 1$ and $\Delta_n = -90°$ (QWR) at discrete angles ϕ_1 in the range $45° < \phi_1 < 90°$. Figures 12 and 13 show the solutions ζ_1 and ζ_2 plotted vs ϕ_1. Table V summarizes QWR design results for the three angles of incidence 52, 75, and 85°. From Figs. 12 and 13 we see that multiple solutions of the same number at a specific ϕ_1 exist in the same ranges as those found for the $\Delta_n = 90°$ QWR. A near-inverse relation exists between the solution branches of these figures and the corresponding ones in Figs. 8 and 9, i.e., $\zeta_{1A}(+90°) + \zeta_{1A}(-90°) \simeq 1$ etc., again due to the symmetry of the CAIC as discussed in Sec. III. For each thickness solution that leads to a net relative phase shift $\Delta_n = 90°$, there exists a corresponding solution that makes $\Delta_n = -90°$.

Figure 14 gives a plot of $\mathcal{R}_{vn}$ vs ϕ_1 for the solution pairs of Figs. 12 and 13. This is nearly an exact copy of Fig. 10, as is also seen by comparing the corresponding entries of $\mathcal{R}_{vn}$ in Tables III and V.

Table VI shows the magnitude and phase errors caused by $\Delta d_i = \pm 1$-nm thickness errors and $\Delta\phi_i = \pm 0.5°$ angle-of-incidence errors. These errors are nearly the same as the corresponding errors shown in Table IV. Again we see a general increase in these errors with ϕ_1. And these errors also vary essentially linearly with Δd_i between ±1 nm and with $\Delta\phi_i$ between ±0.5°.

Figure 15 shows the magnitude and phase errors that result when the wavelength λ varies in the range 10 μm $\leq \lambda \leq$ 11 μm for solution A at $\phi_1 = 75°$, with material dispersion again neglected. The phase error stays below 15%, and the magnitude error is <1%.

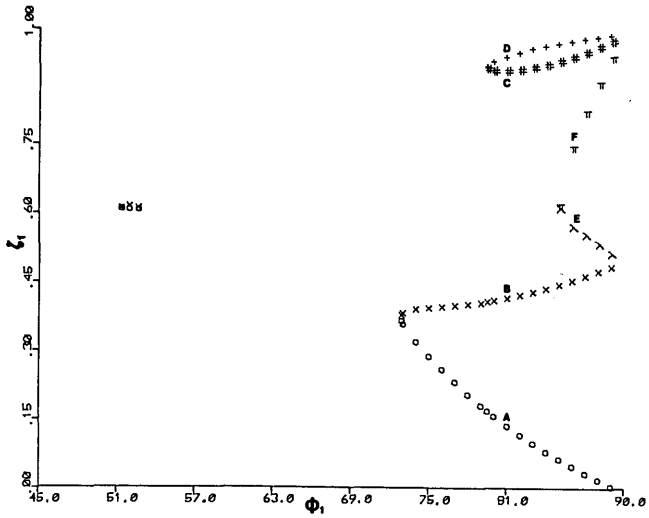

Fig. 12. Normalized film thickness ζ_1 required for QWR ($|\rho_n| = 1$, $\Delta_n = -90°$) vs angle of incidence ϕ_1 (deg) in a ZnS–Ag three-reflection system at $\lambda = 10.6\ \mu m$.

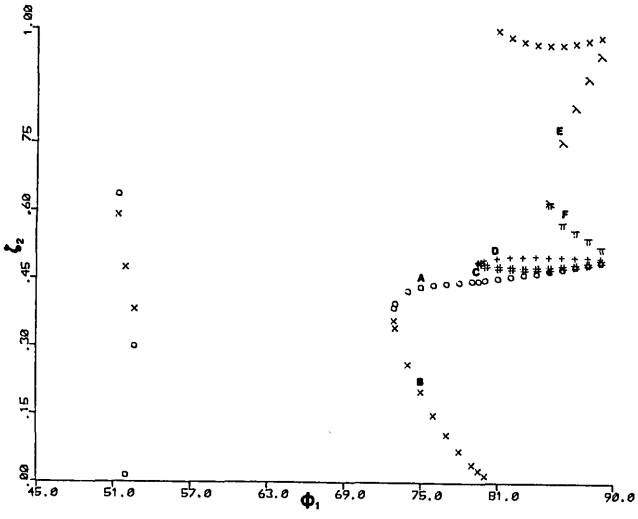

Fig. 13. Same as in Fig. 12 for the associated normalized film thickness ζ_2.

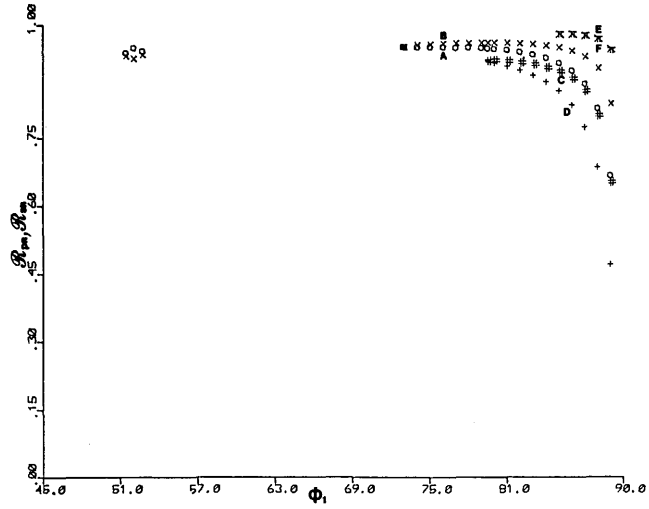

Fig. 14. Net intensity reflectances $\mathcal{R}_{pn} = \mathcal{R}_{sn}$ associated with the design solution pairs (ζ_1,ζ_2) of Figs. 12 and 13.

Table VI. Magnitude and Phase Errors Caused by Introducing (I) Film-Thickness Errors ($\Delta d_1 = \Delta d_2 = \pm 1$ nm), (II) Angle-of-Incidence Errors ($\Delta\phi_1 = \Delta\phi_2 = \Delta\phi_3 = \pm 0.5°$) to the QWR Designs of Table V

Error type	ϕ_1 (deg)	Magnitude error $(\|\rho_n\| - 1) \times 10^4$ −	+	Phase error $[\Delta_n - (-90°)]$ (deg) −	+
I	52 *A*	0.600	−0.598	−0.0537	0.0525
	B	0.536	−0.534	−0.0561	0.0550
	75 *A*	−1.069	1.070	−0.0802	0.0823
	B	−1.086	1.097	−0.0656	0.0677
	85 *A*	−7.450	7.509	−0.1615	0.1754
	B	−2.898	2.965	−0.0881	0.0940
	C	−3.931	3.968	−0.2024	0.2112
	D	5.385	−5.588	−0.3104	0.3006
	E	0.547	−0.543	−0.0339	0.0328
	F	0.547	−0.543	−0.0339	0.0329
II	52 *A*	−0.087	0.087	−2.0732	2.1074
	B	−0.497	0.519	−2.0382	2.0706
	75 *A*	−2.882	3.002	5.1651	−5.2389
	B	1.468	−1.553	4.9799	−5.0454
	85 *A*	−4.030	7.251	14.0157	−15.2209
	B	24.287	−25.924	5.5888	−5.5821
	C	0.643	2.541	−8.0727	9.2161
	D	20.129	−24.842	−7.1972	8.5240
	E	0.034	−0.044	−6.6091	6.6386
	F	−0.139	0.128	−6.5987	6.6281

Table V. Summary of Design Results for ZnS–Ag Three-Reflection Quarterwave Retarders with *s* Fast Axis (QWR: $|\rho_n| = 1$, $\Delta_n = \delta_{pn} - \delta_{sn} = -90°$) at Three Angles of Incidence and at Wavelength $\lambda = 10.6\ \mu m$ [a]

ϕ_1	ζ_1	ζ_2	$D_{\phi 1}$	$D_{\phi 2}$	$\mathcal{R}_{vn}$	δ_{pn}	δ_{sn}
52 *A*	0.60610	0.01252	2.5751	2.4238	0.9520	−119.719	−29.719
B	0.61135	0.47032	2.5751	2.4238	0.9283	74.730	164.730
75 *A*	0.28732	0.43199	2.6814	2.6207	0.9538	−55.083	34.917
B	0.39292	0.19710	2.6814	2.6207	0.9620	−20.116	69.884
85 *A*	0.06262	0.46531	2.7020	2.6941	0.9185	−6.017	83.983
B	0.44122	0.96412	2.7020	2.6941	0.9542	28.667	118.667
C	0.93216	0.47129	2.7020	2.6941	0.9010	−16.303	73.697
D	0.96696	0.49627	2.7020	2.6941	0.8580	−108.245	−18.245
E	0.61142	0.61570	2.7020	2.6941	0.9832	139.889	−130.111
F	0.61542	0.61130	2.7020	2.6941	0.9832	139.940	−130.060

[a] See footnote of Table I for explanation of notation.

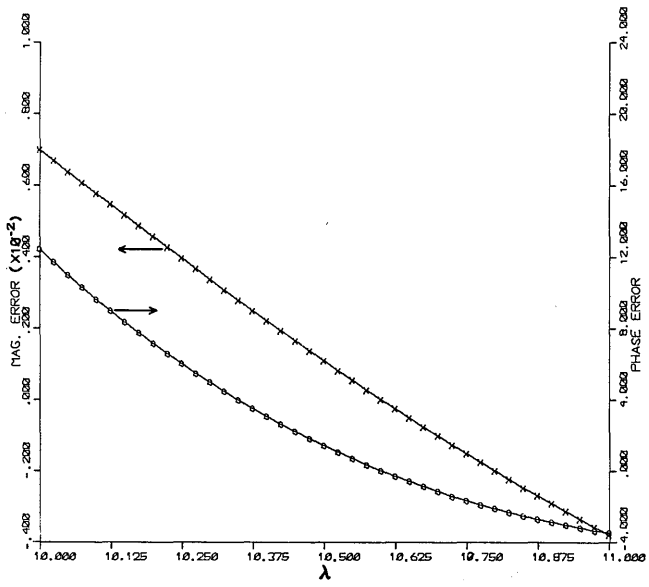

Fig. 15. Magnitude error ($|\rho_n| - 1$) and phase error [$\Delta_n - (-90°)$] caused by wavelength changes in the range 10 μm $\leq \lambda \leq$ 11 μm for solution pair A at $\phi_1 = 75°$ of Table V.

This work was supported by a grant from the State of Louisiana Board of Regents and the Foundation for A Better Louisiana.

V. Summary

In this paper we have described in detail a procedure for the design of three-reflection (three-mirror) film–substrate systems with any desired ratio of net complex p and s reflection coefficients, hence any desired transformation of polarization. Examples are given of halfwave and quarterwave retarders that use ZnS-coated Ag mirrors at the CO_2-laser wavelength $\lambda = 10.6$ μm. The results appear graphically and in tables. The sensitivity to small film-thickness (±1-nm) and angle-of-incidence (±0.5°) errors is determined. Also specific designs have been tested for satisfactory operation over the wavelength range 10 μm $\leq \lambda \leq$ 11 μm.

References

1. R. M. A. Azzam and N. M. Bashara, *Ellipsometry and Polarized Light* (North-Holland, Amsterdam, 1977), p. 371.
2. R. M. A. Azzam, A. R. M. Zaghloul, and N. M. Bashara, "Ellipsometric Function of a Film–Substrate System: Applications to the Design of Reflection-Type Optical Devices and to Ellipsometry," J. Opt. Soc. Am. **65,** 252 (1975).
3. A. R. M. Zaghloul, R. M. A. Azzam, and N. M. Bashara, "Design of Film–Substrate Single-Reflection Retarders," J. Opt. Soc. Am. **65,** 1043 (1975).
4. A. R. M. Zaghloul, R. M. A. Azzam, and N. M. Bashara, "An Angle-of-Incidence Tunable, SiO_2–Si (Film–Substrate) Reflection Retarder for the UV Mercury Line $\lambda \doteq 2537$ Å," Opt. Commun. **14,** 260 (1975).
5. A. R. M. Zaghloul, R. M. A. Azzam, and N. M. Bashara, "SiO_2–Si Film–Substrate Reflection Retarders for Different Mercury Spectral Lines," Opt. Eng. **17,** 180 (1978).
6. S. Kawabata and M. Suzuki, "MgF_2–Ag Tunable Reflection Retarder," Appl. Opt. **19,** 484 (1980).
7. R. M. A. Azzam and M. E. R. Khan, "Single-Reflection Film–Substrate Halfwave Retarders with Nearly Stationary Reflection Properties over a Wide Range of Incidence Angles," J. Opt. Soc. Am. **73,** 160 (1983).
8. W. H. Southwell, "Multilayer Coatings Producing 90° Phase Change," Appl. Opt. **18,** 1875 (1979).
9. J. H. Apfel, "Graphical Method to Design Multilayer Phase Retarders," Appl. Opt. **20,** 1024 (1981).
10. J. H. Apfel, "Phase Retardance of Periodic Multilayer Mirrors," Appl. Opt. **21,** 733 (1982).
11. R. M. A. Azzam and N. M. Bashara, *Ellipsometry and Polarized Light* (North-Holland, Amsterdam, 1977), Sec. 4.3.
12. R. M. A. Azzam and M. E. R. Khan, "Polarization-Preserving Single-Layer-Coated Beam Displacers and Axicons," Appl. Opt. **21,** 3314 (1982).
13. G. W. Stagg and A. H. El-Abiad, *Computer Methods in Power System Analysis* (McGraw-Hill, New York, 1968), p. 249.